nature nanotechnology

LETTERS

PUBLISHED ONLINE: 18 DECEMBER 2011 | DOI: 10.1038/NNANO.2011.224

High-dynamic-range magnetometry with a single nuclear spin in diamond

G. Waldherr[1]*, J. Beck[1], P. Neumann[1], R. S. Said[2,3], M. Nitsche[1], M. L. Markham[4], D. J. Twitchen[4], J. Twamley[2], F. Jelezko[1,5] and J. Wrachtrup[1]

Sensors based on the nitrogen-vacancy defect in diamond are being developed to measure weak magnetic and electric fields at the nanoscale[1–5]. However, such sensors rely on measurements of a shift in the Lamor frequency of the defect, so an accumulation of quantum phase causes the measurement signal to exhibit a periodic modulation. This means that the measurement time is either restricted to half of one oscillation period, which limits accuracy, or that the magnetic field range must be known in advance. Moreover, the precision increases only slowly (as $T^{-0.5}$) with measurement time T (ref. 3). Here, we implement a quantum phase estimation algorithm[6–8] on a single nuclear spin in diamond to combine both high sensitivity and high dynamic range. By achieving a scaling of the precision with time to $T^{-0.85}$, we improve the sensitivity by a factor of 7.4 for an accessible field range of 16 mT, or, alternatively, we improve the dynamic range by a factor of 130 for a sensitivity of 2.5 μT Hz$^{-1/2}$. Quantum phase estimation algorithms have also recently been implemented using a single electron spin in a nitrogen-vacancy centre[9]. These methods are applicable to a variety of field detection schemes, and do not require quantum entanglement.

The basic principle of Larmor frequency-based magnetic field sensing is Ramsey interferometry: a superposition of two appropriate states is created and their field-dependent energy difference is measured by monitoring the evolution of the corresponding phase $\phi \propto B\tau$, where B is the magnetic field and τ is the phase accumulation/sensing time (Fig. 1c). A typcial measurement signal is shown in Fig. 2a. The highest sensitivity δB is reached with the longest phase accumulation/sensing times, $\tau = T_2^*$ (ref. 3). However, approximately 20 oscillations have already occurred up to $\tau = T_2^*$ (that is, $\phi \notin [-\pi/2, \pi/2)$), which go unnoticed when sensing only at $\tau = T_2^*$. Thus, the estimation of B is ambiguous. To prevent this, τ has to be restricted so that $B\tau \propto \phi \in [-\pi/2, \pi/2)$. This leads to an accessible field range of $[-\Delta B_{\max}, \Delta B_{\max})$. As an example, a sensitivity $\delta B = 4.2$ nT Hz$^{-1/2}$ has been demonstrated for the nitrogen vacancy (NV)[4], but the field had to be known before the measurement as $B \in [-31\text{ nT}, 31\text{ nT})$. If this prior information about the magnetic field is not available, estimation of B cannot be performed. To summarize, shorter phase accumulation times τ lead to a broader accessible field range $2\Delta B_{\max} \propto 1/\tau$, but at the same time reduce the sensitivity $\delta B \propto 1/\sqrt{\tau}$.

In a practical measurement application the sensing time τ has to be set by the prior knowledge of the field, and defines the accessible field range of the sensor. By repeating such a measurement n times, the precision is limited by shot noise to $\sigma_B \propto 1/\sqrt{T}$, where $T = n\tau$ is the total sensing time. Here, we apply a recently proposed quantum phase estimation algorithm[8] (QPEA) to a solid-state spin. For a certain accessible field range (16 mT in our case), this algorithm features improved scaling of the precision with measurement time. Effectively, the novel scheme increases the dynamic range of the measurement (that is, $\Delta B_{\max}/\delta B$), and therefore features direct practical benefits for a broad range of frequency metrologies.

The NV$^-$ centre is a favourable system for quantum engineering and measurement techniques[2,3,5] because of its optical spin polarization and readout mechanism[10], long coherence times[4], even at ambient conditions, and coherent coupling to nearby nuclear spins[11,12]. Its highly confined spin density allows field sensing at a nanometre scale[1]. Recently, the facility for quantum non-demolition (QND) measurements allowing single-shot readout has been added to these features[13,14]. In this work, we use QND measurement to demonstrate improved magnetic field sensing with the nitrogen nuclear spin, following ref. 8. The NV electron spin is used to correct for unwanted magnetic field fluctuations by optically detected magnetic resonance[15], to measure the pure statistical variance of the algorithm (see Supplementary Information).

The experiment was carried out on a natural ^{14}NV$^-$ in isotopically pure (^{12}C > 99.99%) chemical vapour deposition diamond. Figure 1a shows the structure of the NV in the diamond lattice. The magnetic moment associated with the nuclear (and electron) spin leads to a magnetic field-dependent energy shift of the different spin states (Fig. 1b). This Zeeman shift $\omega = \gamma_n B$ of the spin states can be measured by Ramsey interferometry (see Methods and Fig. 2c) through the quantum phase $\phi(\tau) = \omega\tau$. Figure 2a,b shows the Ramsey fringes of the nuclear spin. Eventually, we can deduce the field offset B from the measured phase.

For this approach, the precision σ_B of n independent measurements with phase accumulation time τ scales as $1/(\tau\sqrt{n})$ (according to the central limit theorem), corresponding to the $1/\sqrt{T}$ limit, where $T = n\tau$. For a single measurement with phase sensing time $n\tau$, however, we achieve $\sigma_B \propto 1/(\tau n)$, corresponding to the $1/T$ limit (Fig. 1d). Consequently, it is desirable to make $n\tau$ as large as possible for a single measurement, which, however, will make the phase measurement ambiguous if $\phi \notin [-\pi/2, \pi/2)$. Because $\phi = \gamma_n B\tau$, the maximum expected magnetic field range $[-\Delta B_{\max}, \Delta B_{\max})$ limits the longest phase accumulation time to

$$\tau_0 < \frac{\pi}{2\gamma_n \Delta B_{\max}} \qquad (1)$$

for the measurement to be unambiguous. Hence, we define τ_0 as one resource.

To achieve both unambiguous field measurements and high sensitivity, weighted measurements for different values of $\tau \geq \tau_0$ are

[1]3. Physikalisches Institut, Research Center SCOPE, and MPI for Solid State Research, University of Stuttgart, Pfaffenwaldring 57, 70569 Stuttgart, Germany, [2]Centre for Engineered Quantum Systems, Department of Physics & Astronomy, Faculty of Science, Macquarie University, Sydney, NSW 2109, Australia, [3]Institut für Quanten-Informationsverarbeitung, Universität Ulm, 89081 Ulm, Germany, [4]Element Six Ltd, King's Ride Park, Ascot SL5 8BP, UK, [5]Institut für Quantenoptik, Universität Ulm, 89073 Ulm, Germany. *e-mail: g.waldherr@physik.uni-stuttgart.de

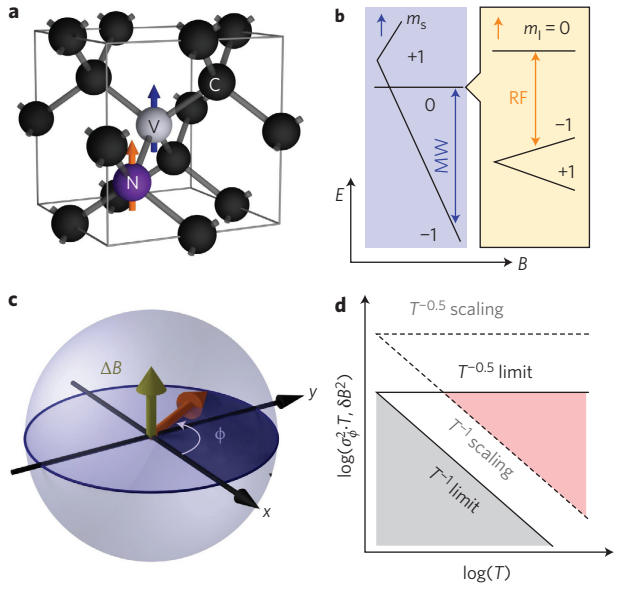

Figure 1 | NV centre spins in an external magnetic field. a, Structure of the NV inside the diamond lattice (C, carbon; N, nitrogen; V, vacancy). The blue and orange arrows indicate the electron and nitrogen nuclear spins, respectively. **b**, Energy-level scheme and magnetic field dependence of the NV^- ground-state spin triplet. The magnification shows the ^{14}N hyperfine structure in the $m_S = 0$ state. The arrows indicate the transitions, which are addressed in the experiment. **c**, Bloch sphere illustrating the nuclear spin state (orange arrow), as it precesses around the magnetic field ΔB and thereby accumulates the phase ϕ. **d**, Qualitative graph showing the $1/\sqrt{T}$ and $1/T$ limits. Note that the vertical axis is the phase variance σ_ϕ^2 multiplied by the total phase accumulation time T. Dashed lines show the possible scaling of an experiment, which scales as the corresponding limit but does not reach it due to measurement errors.

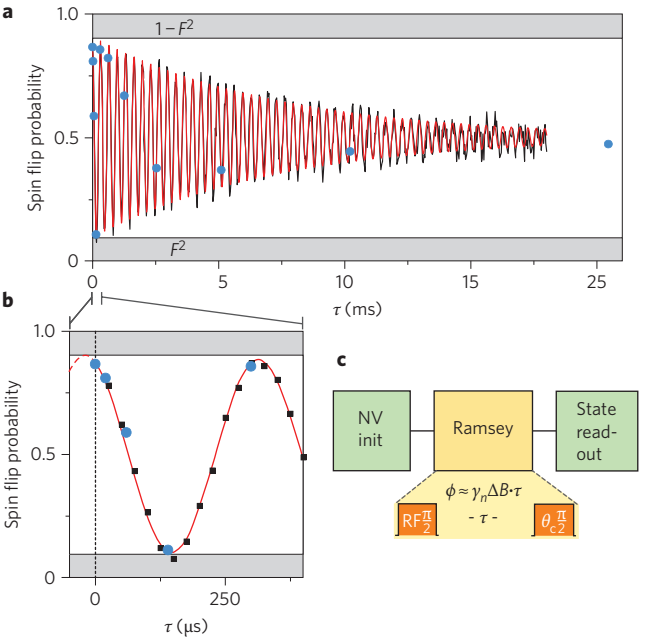

Figure 2 | Ramsey interferometry using a single spin. a, Ramsey fringes of the nitrogen nuclear spin. The black line shows the measurement results, the red line a decaying cosine fit, and the blue dots the measurement points of the QPEA. The contrast of the fringes is reduced due to the limited fidelity (F) of the state measurement, which occurs twice: for initialization and readout. The exponential decay is due to coherence loss with a time constant $T_2^\star \approx 7.25$ ms (dominated by T_1 decay of the NV electron spin). For a single measurement point with long phase accumulation time, the number of fringes will be unknown; that is, the phase/frequency measurement is ambiguous. **b**, Magnification of the Ramsey fringes for small times. The fit reveals the phase that is accumulated even for a waiting time $\tau = 0$, which leads to an offset of 20 μs (see Methods). **c**, Pulse sequence for Ramsey interferometry. See Supplementary Information for details.

performed. In addition, a controlled phase shift θ_c is needed to determine ϕ modulo 2π. This control phase can either be set adaptively with a feedback algorithm, or non-adaptively with a pre-set sequence of phase shifts[8]. For technical reasons, we use the non-adaptive QPEA. The phase sensing times are $\tau_k = \tau_0 2^k$, where $k = 0, 1, 2, \ldots, K$, and the weighting is carried out by setting the number of repetitions for each τ_k as

$$M_{(K,k)} = M_K + F(K - k) \tag{2}$$

(Fig. 3a). The total phase sensing time is

$$T = \tau_0 \sum_{k=0}^{K} M_{(K,k)} \times 2^k \tag{3}$$

and the total number of resources is $N = T/\tau_0$. The optimal choice of the integer weighting parameters M_K and F can be determined by simulations[8]. In our case, we chose $M_K = 36$ and $F = 8$. We use $\tau_0 = 20$ μs for our measurements. In general, τ_0 must be chosen so that the measurement only yields results (is sensitive) if the magnetic field is within the above defined limits (see Supplementary Information). With this scheme, unambiguous, near $1/T$ scaled phase estimation can be achieved, while the linewidth of the transition frequency (which is related to the $T_2^\star$ time) limits the achievable precision.

The result of one single phase accumulation (one application of the sequence shown in Fig. 2c) will either yield $m_I = 0$ or $m_I = -1$, corresponding to a 0 or 1, respectively, for the Ramsey fringes shown in Fig. 2a. Each such result yields a probability distribution for the phase (see ref. 8 for details), which depends on the waiting time τ_k, the contrast of the Ramsey fringes (79% in our case) and the coherence time $T_2^\star$ (~7.25 ms). One complete run of the QPEA comprises single phase accumulations for increasing τ_k, each repeated $M_{(K,k)}$ times. For the final result the probability distributions of all these single phase accumulations are multiplied and the most likely phase is the estimate. Figure 3c shows such a probability distribution of a single run of the QPEA, and how it emerges from increasing the total phase accumulation time T by increasing k. To measure the variance σ_ϕ^2 of this estimate, the entire QPEA is run many times and the variance of the results is calculated, as illustrated in Fig. 3b.

We now analyse the scaling of the variance σ_B^2 of the magnetic field measurement on the total phase accumulation time T. Therefore, T is increased by increasing the parameter K in equation (2) (that is, by allowing longer single sensing times up to τ_K). As in ref. 8, we display $\sigma_B^2 T$ (corresponding to the squared magnetic field sensitivity δB^2) versus T (Fig. 4a):

$$\delta B = \sqrt{\sigma_B^2 T}, \qquad \sigma_B = \frac{\sigma_\phi}{\gamma_n \tau_0} \tag{4}$$

We then compare the precision scaling of the QPEA with the standard measurement approach by repeating the measurements for a sensing time τ_0. Figure 4a shows the result of this measurement. As expected, the standard measurement shows a scaling of $1/\sqrt{T}$, which translates into a horizontal line in Fig. 4a, that is, a constant value for δB^2. The vertical offset to the ideal case is mainly due to

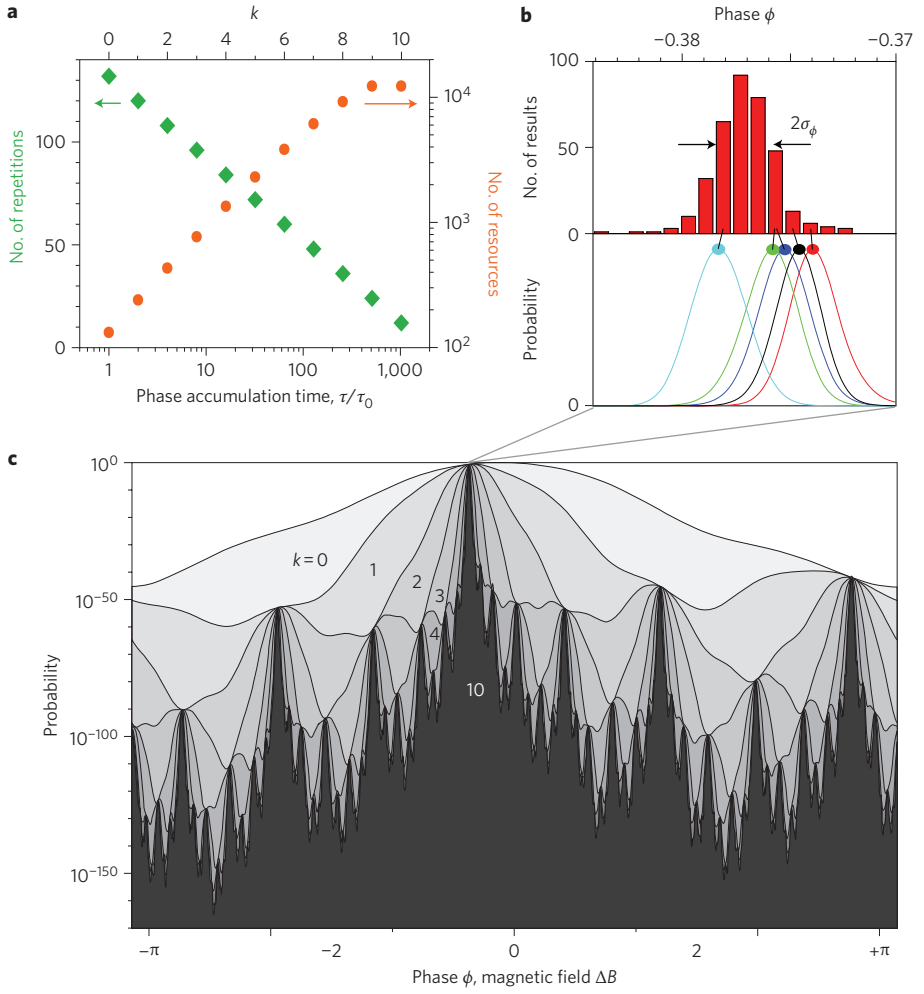

Figure 3 | Quantum phase estimation algorithm. a, Number of measurement repetitions $M_{(K,k)}$ and number of used resources $N_{(K,k)} = M_{(K,k)} \times 2^k$ for each phase accumulation time $\tau_k/\tau_0 = 2^k$. The total number of resources and total phase accumulation time are $N = \sum_k N_{(K,k)}$ and $T = N\tau_0$, respectively. **b**, Bottom: resulting probability distributions of five individual runs of the QPEA. The maximum of each distribution yields the corresponding phase estimate. Top: histogram of phase estimates, which is used to determine the phase variance σ^2_ϕ. **c**, Evolution of a typical probability distribution for the estimated phase ϕ and corresponding magnetic field ΔB during one run of the QPEA. The probability is shown after all measurements for each $k = 0, 1, \ldots, K$, $K = 10$. Measurements with $k = 0$ remove the ambiguity but have a comparatively high variance. As k is increased (darker shaded regions) the measurements yield a smaller variance (sharper peaks) but also introduce ambiguity (more peaks). The overall probability distribution has an unambiguous maximum.

the reduced fidelity of the spin state readout. The precision scaling of the QPEA, however, is close to $1/T$. The offset of the QPEA to the $1/T$ limit results from the additional measurements needed to remove the ambiguity.

The gain in sensitivity of the QPEA compared to the standard measurement depends on prior knowledge of the maximum magnetic field $\Delta B_{\max}$. Figure 4b shows the sensitivity of the standard and the QPEA measurement approach as a function of $\Delta B_{\max}$, where τ_0 is chosen according to equation (1). As can be seen, the sensitivity of the standard measurement becomes worse with increasing $\Delta B_{\max}$. This is related to the decrease of phase sensing time τ, which in turn deteriorates $\delta B \propto 1/\sqrt{\tau}$. The sensitivity of the QPEA, however, hardly changes with increasing $\Delta B_{\max}$. For a completely known magnetic field, that is, for smallest $\Delta B_{\max}$, the dynamic range of the standard measurement with longest $\tau_0 = T_2^*$ is sufficient to achieve the highest sensitivity and to be unambiguous at the same time. If, however, the prior knowledge about the magnetic field decreases, that is, $\Delta B_{\max}$ increases, the dynamic range of the standard measurement is too small to maintain the highest sensitivity while staying unambiguous at the same time. Hence, the sensitivity decreases. Obviously, the dynamic range of the QPEA measurement increases for increasing $\Delta B_{\max}$ in such a way that the sensitivity remains almost unaltered.

To conclude, we have demonstrated improved magnetic field sensing based on quantum phase estimation, which shows $T^{-0.85}$ scaling, and increases the dynamic range of the sensor by over two orders of magnitude compared to a standard measurement due to the unambiguous, high-precision measurements. This will become even more important for future improvements in the coherence times of field sensors, because the accessible field range of the standard measurement scales inversely with the phase accumulation time. Although our experiment was carried out on the nitrogen nuclear spin to demonstrate the basic principle, the electron spin would be more suitable for field sensing due to its higher magnetic moment (~9,000 times). Furthermore, the electron spin of the NV can also be used to detect electric fields[5]. The techniques presented here can be applied directly to the electron spin: after initialization of the nuclear spin and electronic state, the electron spin state can easily be mapped onto the nuclear spin state, which can then be measured in a single shot. Similar improvements in field sensing with the NV electron spin without single-shot readout have also been achieved[9].

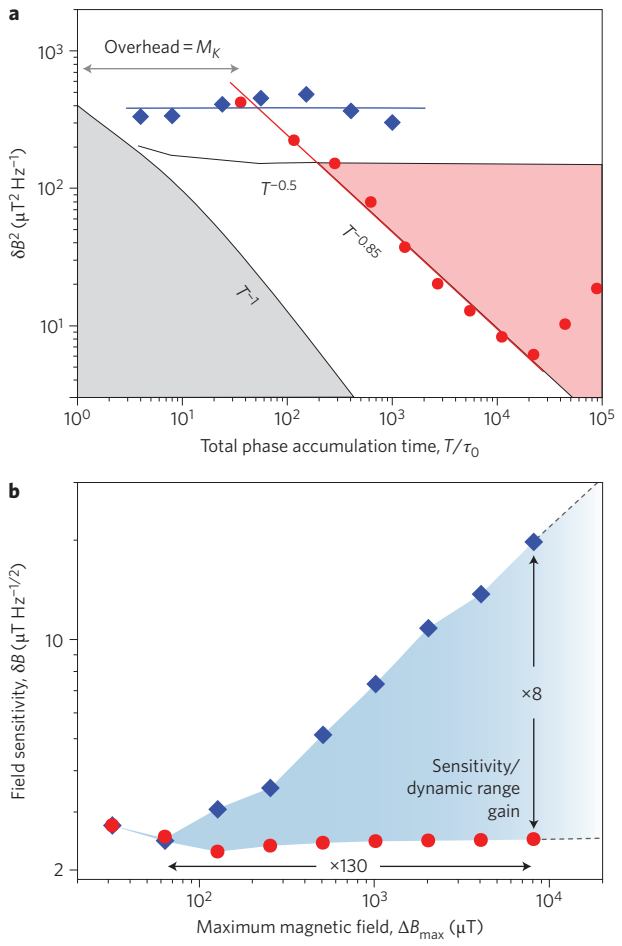

Figure 4 | Comparison of QPEA and the standard measurement scheme. **a**, Precision scaling of the QPEA (red dots, calculated from 358 runs of the algorithm; Fig. 3) compared to the standard measurement (blue diamonds). The magnetic field variance σ_B^2 multiplied by the total phase accumulation time is shown as a function of the total phase accumulation time. The limited readout fidelity leads to a constant offset of the standard measurement compared to the $1/\sqrt{T}$ limit (numerical calculation for ideal parameters: 100% fidelity and no decay). The QPEA has the same vertical offset and an additional horizontal one because of the measurement overhead. The precision scaling of the QPEA is $T^{-0.85}$, and surpasses the $1/\sqrt{T}$ limit. As can be seen, for phase accumulation times larger than the T_2^* time (=7.25 ms, the last two points are for $\tau_k \approx 10$ and 20 ms), no further information on the magnetic field can be obtained, while the total phase accumulation time is increased, which leads to the increase of δB^2. The analytical expression for the $1/T$ limit is taken from ref. 17. **b**, Dependence of the sensitivity of the standard measurement (blue diamonds) and the QPEA (red dots) on previous knowledge of the maximum magnetic field. The blue area indicates the gain of the dynamic range and sensitivity of the QPEA compared to the standard measurement.

Methods

To perform Ramsey interferometry, the state of the nuclear spin is initialized by single-shot readout (see Supplementary Information). The electronic state of the NV must also be initialized; it has been shown that the NV can be photo-ionized, leaving it in the neutral charge state NV^0 with 30% probability[16]. In this case, radiofrequency (RF) pulses aimed for the nuclear spin transitions in NV^- will have no effect. We used a post-selection technique (shown in the Supplementary Information) for initializing the correct electronic state.

To create the superposition state $|0\rangle + |1\rangle$ of the nuclear spin, an (off-resonant) RF $\pi/2$ pulse (corresponding to the $m_I = -1 \leftrightarrow 0$ transition) is applied, which rotates the nuclear spin state by 90° around the x-axis on the Bloch sphere. In the rotating frame of the RF, the field vector of the RF remains constant, whereas the superposition state precesses in the x–y plane on the Bloch sphere, with a frequency $\omega = \gamma_n \Delta B$ corresponding to the detuning; that is, $\omega = \omega_{rf} - \omega_{m_I=0\leftrightarrow-1}$. Therefore, the phase ϕ of this superposition state $|0\rangle + e^{i\phi}|1\rangle$ increments as $\phi_{(t)} = \omega t$. After waiting for a certain amount of time τ, a second RF $\pi/2$ is applied, which again rotates the spin state by 90° around the x-axis on the Bloch sphere, thereby mapping the accumulated phase onto the population of the $m_I = 0, -1$ states, which can then be measured (Fig. 2c).

The control phase θ_c, needed for the QPEA, is applied by changing the phase of the second RF $\pi/2$ pulse, which sets the rotation axis in the x–y plane of the Bloch sphere. We used four control phases $\theta_c = \{0, \pi/2, \pi, 3\pi/2\}$, corresponding to rotations on the Bloch sphere around the axes $\{x, y, -x, -y\}$. The detailed pulse sequence, including the post-selection for the electronic state, is shown in the Supplementary Information.

Because of the finite length of the RF pulses, the phase is already starting to accumulate during the application of the pulses; that is, the measured phase at $\tau = 0$ is not 0, and actually depends on the frequency offset ω. However, for rectangular-shaped pulses and small detuning, this phase corresponds to an additional, fixed phase accumulation time ϵ, which can be corrected by using the time $\tau' = \tau + \epsilon$ when calculating the frequency $\Delta\omega = \phi/\tau'$. Here, $\epsilon = 20$ μs. In this work, we omit the dash (τ') for simplicity and denote the corrected phase accumulation time as τ.

Received 12 September 2011; accepted 16 November 2011; published online 18 December 2011

References

1. Balasubramanian, G. *et al.* Nanoscale imaging magnetometry with diamond spins under ambient conditions. *Nature* **455,** 648–651 (2008).
2. Maze, J. R. *et al.* Nanoscale magnetic sensing with an individual electronic spin in diamond. *Nature* **455,** 644–647 (2008).
3. Taylor, J. M. *et al.* High-sensitivity diamond magnetometer with nanoscale resolution. *Nature Phys.* **4,** 810–816 (2008).
4. Balasubramanian, G. *et al.* Ultralong spin coherence time in isotopically engineered diamond. *Nature Mater.* **8,** 383–387 (2009).
5. Dolde, F. *et al.* Electric-field sensing using single diamond spins. *Nature Phys.* **7,** 459–463 (2011).
6. Higgins, B. L., Berry, D. W., Bartlett, S. D., Wiseman, H. M. & Pryde, G. J. Entanglement-free Heisenberg-limited phase estimation. *Nature* **450,** 393–396 (2007).
7. Higgins, B. L. *et al.* Demonstrating Heisenberg-limited unambiguous phase estimation without adaptive measurements. *New J. Phys.* **11,** 073023 (2009).
8. Said, R. S., Berry, D. W. & Twamley, J. Nanoscale magnetometry using a single-spin system in diamond. *Phys. Rev. B* **83,** 125410 (2011).
9. Nusran, N. M., Momeen, U. & Dutt, M. V. G. High dynamic range magnetometry with a single electron spin in diamond. *Nature Nanotech.* http://dx.doi.org/10.1038/nnano.2011.225 (2011).
10. Gruber, A. *et al.* Scanning confocal optical microscopy and magnetic resonance on single defect centers. *Science* **276,** 2012–2014 (1997).
11. Jelezko, F. *et al.* Observation of coherent oscillation of a single nuclear spin and realization of a two-qubit conditional quantum gate. *Phys. Rev. Lett.* **93,** 130501 (2004).
12. Childress, L. *et al.* Coherent dynamics of coupled electron and nuclear spin qubits in diamond. *Science* **314,** 281–285 (2006).
13. Neumann, P. *et al.* Single-shot readout of a single nuclear spin. *Science* **329,** 542–544 (2010).
14. Buckley, B. B., Fuchs, G. D., Bassett, L. C. & Awschalom, D. D. Spin-light coherence for single-spin measurement and control in diamond. *Science* **330,** 1212–1215 (2010).
15. Steiner, M., Neumann, P., Beck, J., Jelezko, F. & Wrachtrup, J. Universal enhancement of the optical readout fidelity of single electron spins at nitrogen-vacancy centers in diamond. *Phys. Rev. B* **81,** 035205 (2010).
16. Waldherr, G. *et al.* Dark states of single nitrogen-vacancy centers in diamond unraveled by single shot NMR. *Phys. Rev. Lett.* **106,** 157601 (2011).
17. Berry, D. W. *et al.* How to perform the most accurate possible phase measurements. *Phys. Rev. A* **80,** 052114 (2009).

Acknowledgements

The authors thank C. Wunderlich for providing a versatile frequency generator (VFG-150). This work was supported by ERC Project SQUTEC, the DFG SFB/TR21 and EU Projects DIAMANT and SOLID.

Author contributions

G.W., J.B., P.N. and M.N. carried out the experiment. R.S.S., J.B., P.N., G.W., J.T. and F.J. conceived and designed the experiment. M.L.M. and D.J.T. prepared the diamond. G.W., P.N., R.S.S., F.J., J.T. and J.W. wrote and discussed the manuscript. F.J., J.T. and J.W. supervised the project.

Additional information

The authors declare no competing financial interests. Supplementary information accompanies this paper at www.nature.com/naturenanotechnology. Reprints and permission information is available online at http://www.nature.com/reprints. Correspondence and requests for materials should be addressed to G.W.